Ore Geology Reviews 93 (2018) 200–210

Contents lists available at ScienceDirect

Ore Geology Reviews

journal homepage: www.elsevier.com/locate/oregeorev

Recognition of Late Jurassic W-Sn mineralization and its exploration potential on the western margin of the Caledonian Guidong granite batholith, Nanling Range, South China: Geochronological evidence from the Liuyuan Sn and Zhuyuanli W deposits

Yabin Yuan[a], Shunda Yuan[a,*], Jingwen Mao[a], Panlao Zhao[a], Chen Yan[a], Haijie Zhao[a], Dongliang Zhang[b], Yan Shuang[c], Jiantang Peng[b,d]

[a] MLR Key Laboratory of Metallogeny and Mineral Assessment, Institute of Mineral Resources, Chinese Academy of Geological Sciences, Beijing 100037, China
[b] Earth Science & Geophysics Information College of Central South University, Changsha 410083, China
[c] Chongqing Key Laboratory of Exogenic Minerallization and Mine Environment, Chongqing Institute of Geology and Mineral Resources, Chongqing 400042, China
[d] State Key Laboratory of Ore Deposit Geochemistry, Institute of Geochemistry, Chinese Academy of Sciences, Guiyang 550002, China

ARTICLE INFO

Keywords:
Muscovite Ar-Ar
SIMS zircon U-Pb
Potential for W-Sn exploration
Nanling Range

ABSTRACT

Recently, the mineral potential of the area surrounding the granitic batholiths in the Nanling Range was highlighted by the discovery of a series of tungsten and tin deposits or occurrences hosted in or near the Penggongmiao and Guidong batholiths in southern Hunan Province, South China. However, the lack of high-precision geochronological data from these deposits has hampered the understanding of their ore genesis and further W-Sn exploration progress. Based on detailed geological investigations, we obtained precise Secondary Ion Mass Spectroscopy (SIMS) zircon U-Pb and muscovite Ar-Ar ages from the greisen-dominated Liuyuan tin deposit and Zhuyuanli tungsten deposit, which are located on the western margin of the Guidong batholith. The results show that the $^{40}Ar/^{39}Ar$ plateau age of muscovite (153.10 ± 0.96 Ma) from the Liuyuan tin deposit is consistent with the $^{40}Ar/^{39}Ar$ plateau age of muscovite (151.64 ± 0.96 Ma) from the Zhuyuanli tungsten deposit within analytical error. These data indicate that the W-Sn mineralization in the region occurred during the Late Jurassic, which is significantly later than the emplacement of the Caledonian (Early Paleozoic) ore-hosting Guidong granite batholith, as evidenced by the SIMS zircon U-Pb age data from the Liuyuan greisen (438.1 ± 2.6 Ma) and the Zhuyuanli greisenized granite (433.8 ± 3.1 Ma). The remarkable differences in age between the Guidong batholith emplacement and formation of these two W-Sn ore deposits indicate that the regional tungsten and tin mineralization is temporally and genetically associated with possibly concealed Late Jurassic granite at depth rather than with the surrounding Caledonian granite batholith. The uniform W-Sn mineralization age (153–151 Ma) of the Liuyuan and Zhuyuanli deposits suggests that significant Late Jurassic W-Sn ore-forming potential exists along the western margin of the Guidong batholith.

1. Introduction

The Nanling Range, which is located in the central region of South China, is a world-renowned W-Sn metallogenic belt (Mao et al., 2007). It has been widely recognized that the W-Sn mineralization in the Nanling Range is related to granitic rocks (Hua, 2005; Chen et al., 2008; Mao et al., 2008, 2013). Moreover, in most cases, the W-Sn mineralization is genetically related to the late-stage differentiated granites of the granite complex (Mao et al., 2007). Therefore, the definitive establishment of the geochronological framework of the granite emplacement and W-Sn mineralization is of great significance to the study of ore genesis and regional mineral exploration. Previous studies have demonstrated that the Late Jurassic (160–150 Ma) granitic stocks or apophyses exhibit pronounced W-Sn mineralization potential, as indicated by a large number of ore deposits, such as the Xianghualing Sn deposit (Yuan et al., 2007), the Shizhuyuan W-Sn-Mo-Bi deposit (Li et al., 1996), the Yaogangxian W deposit (Peng et al., 2006), the Hongqiling Sn deposit (Yuan et al., 2012a), the Jinchuantang Sn-Bi deposit (Liu et al., 2012), and the Huangshaping Pb-Zn-W-Mo deposit (Yuan et al., 2014). In recent years, a series of W-Sn deposits and occurrences have been found hosted in or near granite batholiths of the Nanling Range (Hua et al., 2013; Chen et al., 2013). It is necessary to

* Corresponding author.
E-mail address: shundayuan@cags.ac.cn (S. Yuan).

https://doi.org/10.1016/j.oregeorev.2017.12.025
Received 29 September 2017; Received in revised form 17 December 2017; Accepted 28 December 2017
Available online 30 December 2017
0169-1368/

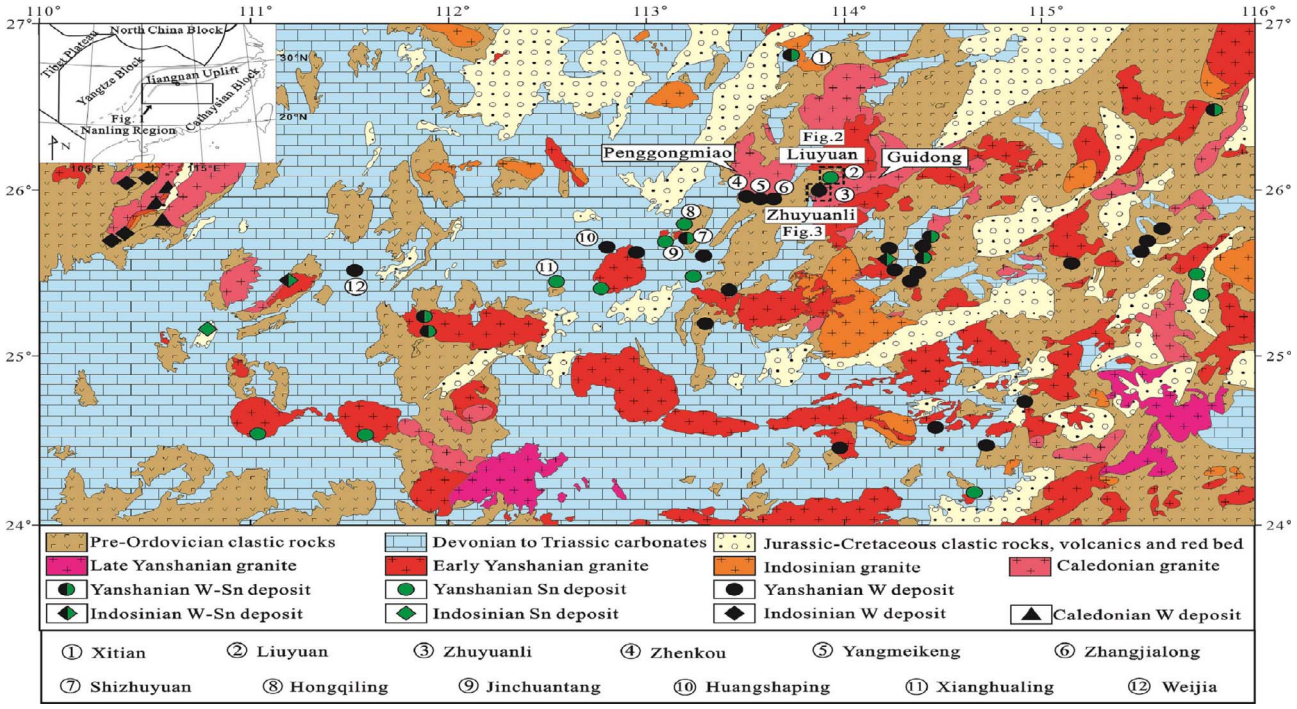

Fig. 1. Map of the distribution of granites and associated tungsten and tin deposits in Nanling Range (Modified after Chen et al., 2013).

constrain the temporal relationships between multi-phase granites and the related W-Sn mineralization for better understanding the genesis of W-Sn deposits and to guide mineral exploration in this region.

The Caledonian Penggongmiao and Guidong granite batholiths, which cover ca. 900 km^2 and over 1000 km^2, respectively, are located in the eastern region of southern Hunan Province (Fig. 1). Recent exploration revealed that a series of W-Sn deposits, such as the Zhangjialong, Zhenkou, Yangmeikeng, and Zhuyuanli tungsten deposits, as well as the Liuyuan tin deposit, are distributed around these two granite batholiths (Fig. 1). These W-Sn deposits have long been believed to have formed during the Caledonian; thus, the prospecting strategy has centred on the Caledonian granites and their contact zones with pre-existing strata (Qiao et al., 2011; Li et al., 2013a). However, the lack of high-precision geochronological data from these W-Sn deposits in the Penggongmiao-Guidong area has hampered the understanding of their ore genesis and further W-Sn exploration progress.

Based on previous studies and a detailed field geological investigation, we performed the systematic in situ SIMS zircon U-Pb and muscovite Ar-Ar dating of samples from the Liuyuan and Zhuyuanli deposits to further understand the ore genesis of these W-Sn deposits around the Guidong batholiths and to evaluate the regional ore-forming potential.

2. Regional geologic setting

The Nanling Range, which is one of the most important W-Sn metallogenic belts in the world, is located in the central region of South China and covers an area of 170,000 km^2 (Chen et al., 2002; Yuan et al., 2011). Tectonically, it is located in the northwestern region of the Cathaysia block (Fig. 1). The regional basement consists of Sinian-Silurian clastic and metamorphic clastic rocks. The overlying sedimentary strata comprise Devonian to Jurassic marine and marine-continental strata, including carbonate rocks, marlstone and clastic beds (Mao et al., 2007). Many small fault basins formed in this area from the Jurassic to the Cretaceous; these basins are filled with clastic rocks, volcanic rocks and red clastic sediments (Mao et al., 2007). The pre-Mesozoic basins were mainly affected by Indosinian tectonic events related to the Tethys regime; they were also affected by the Pacific regime and intra-continental tectonism and magmatism that began during the Cretaceous (Shu and Wang, 2006). These tectono-magmatic events generated a regional basin-mountain system that primarily comprises large volumes of volcanic and granitic rocks. Among these igneous rocks, small highly fractionated granites occurring as stocks or apophyses have been found to show great W-Sn mineralization potential. Moreover, in recent years, the mineral potential of the area surrounding the granite batholiths in the Nanling Range and its adjacent area has been highlighted by the discovery of the world-class Dahutang supergiant tungsten deposit and the large Xitian tin deposit, which are hosted in regional granite batholiths. In southern Hunan Province, recent exploration has also revealed that a series of W-Sn deposits and occurrences are distributed around the regional Penggongmiao and Guidong batholiths (Fig. 1; Qiao et al., 2011; Li et al., 2013a).

3. Geology of the Liuyuan and Zhuyuanli deposits

3.1. The Liuyuan tin deposit

The Liuyuan tin deposit is located in the western margin of the Guidong batholith (Fig. 1). The Cambrian epimetamorphic sandstone that is exposed in the western and northern parts of the deposit, was intruded by the Caledonian Guidong granite batholith and several muscovite granite dykes (Fig. 2). The faults in this area are dominated by well-developed NW- and NE-trending faults (Fig. 2). In addition, a series of NE-trending faults host almost all of the tin veins in the Liuyuan deposit, and control the distribution of the ore bodies. The ore-barren NW-trending faults, which are generally filled with quartz veins, commonly cut the NE-trending faults hosting the tin orebodies, with several meters of offset (Fig. 2).

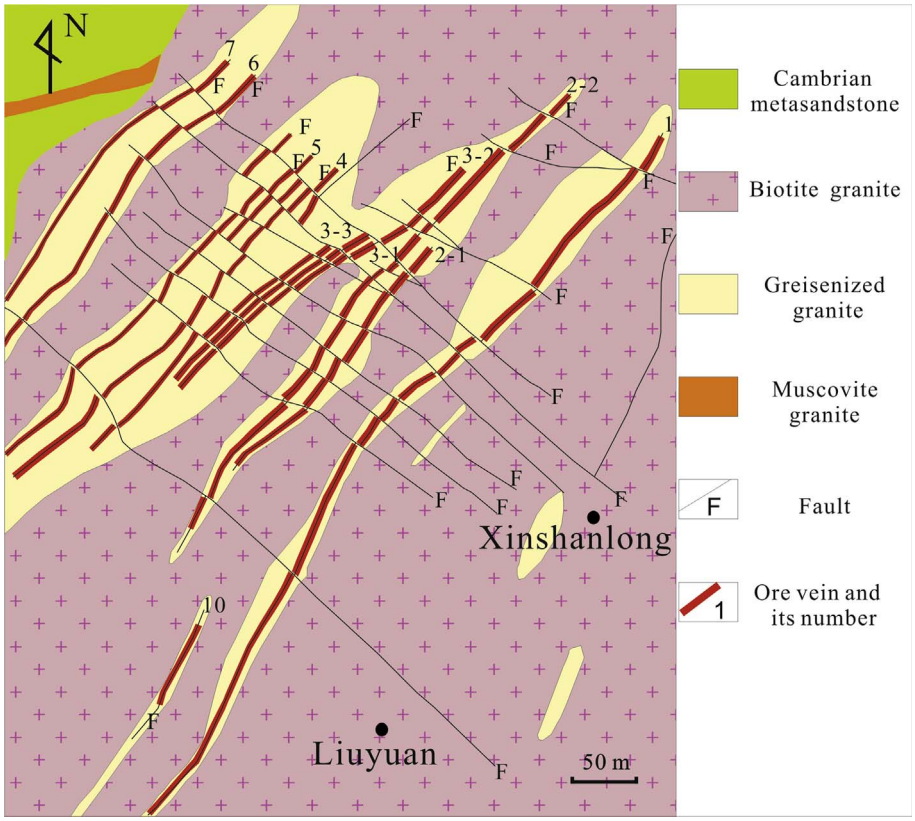

Fig. 2. Geological sketch map of the Liuyuan tin deposit (Modified from Hunan Metallurgical Team of 238. 1977).

The Caledonian granites exhibit a widespread distribution throughout the mining area. The dominant rock type is medium- to coarse-grained biotite granite. These granites (Fig. 5g, h) are commonly grey-white in colour and contain 35–45% quartz, 25–35% K-feldspar, 8–12% plagioclase and 2–5% biotite, as well as trace amounts of muscovite, apatite, zircon and magnetite. The observed hydrothermal alteration types mainly include greisenization, chloritization and silicification (Fig. 5i). Among these, greisen alteration is closely related to tin mineralization. On both sides of the ore-bearing faults, the granite exhibits extensive greisen alteration; this alteration fades with increasing distance from the centre of the faults (Fig. 2), in contrast to the massive greisen alteration occurring in the apical portion of the ore-related granite. Past mining activity has revealed the presence of 14 main orebodies, including quartz-cassiterite veins (Fig. 5d) and greisen-type orebodies (Fig. 5a). The most common ore mineral in these orebodies is cassiterite, accompanied by minor hematite, magnetite, chalcopyrite, sphalerite, galena, arsenopyrite and other minerals. The gangue minerals include quartz, feldspar, muscovite, sericite and chlorite.

3.2. The Zhuyuanli tungsten deposit

The Zhuyuanli tungsten deposit, which is located to the south of the Liuyuan tin deposit, is also located on the western margin of the Guidong batholith. This granite batholith outcrops across almost the entire area of the Zhuyuanli deposit (Fig. 3). The dominant rock type is fine- to medium-grained biotite adamellite, which is generally composed of 30–35% K-feldspar, 30–32% plagioclase, 25–28% quartz and 5–7% biotite, as well as trace amounts of muscovite, hornblende and zircon. Most of the granite in the deposit exhibits varying degrees of hydrothermal alteration (Fig. 5j, k), including greisen alteration, silicification, chloritization and sericitization. The important tungsten mineralization generally co-occurs with well-developed greisen alteration.

The main structures present in the mining area are NE- and NNE-trending faults, as well as some joints (Fig. 3). The NE- and NNE-trending faults, which host the major tungsten veins, control the distribution and structure of the orebodies in the Zhuyuanli deposit (Fig. 3). For example, the typical No. 3 tungsten vein, which is one of the largest orebodies in the area (with an approximate length of 2750 m), is hosted along the NE-trending F_3 fault, as revealed at the spot of LL15 (an old working spot; Figs. 3 and 4). To date, 13 primarily greisen-type orebodies have been found in the Zhuyuanli area. The most common ore mineral in the Zhuyuanli tungsten deposit is wolframite, which is accompanied by other minor minerals such as bismuthinite, scheelite, chalcopyrite, sphalerite, galena and arsenopyrite. The primary gangue minerals are quartz and feldspar and the secondary ones are muscovite, sericite and chlorite.

4. Sampling and analytical procedures

The studied samples were collected from greisen and greisenized granite associated with the Liuyuan tin deposit and the Zhuyuanli tungsten deposit in the Guidong batholith. The zircon grains and one muscovite separate, extracted from the greisenized granite associated with the tungsten mineralization (sample ZYL-1) in the Zhuyuanli deposit, were used for U-Pb and Ar-Ar dating, respectively. Samples LY-9 and LY-11,which were both obtained from the greisen related to the tin mineralization in the Liuyuan deposit, were processed to obtain zircon grains for U-Pb dating and one muscovite separate for Ar-Ar dating. These mineral grains were separated using the application of standard heavy liquid and magnetic techniques, followed by hand picking under a binocular microscope. These procedures were conducted at Chengxin

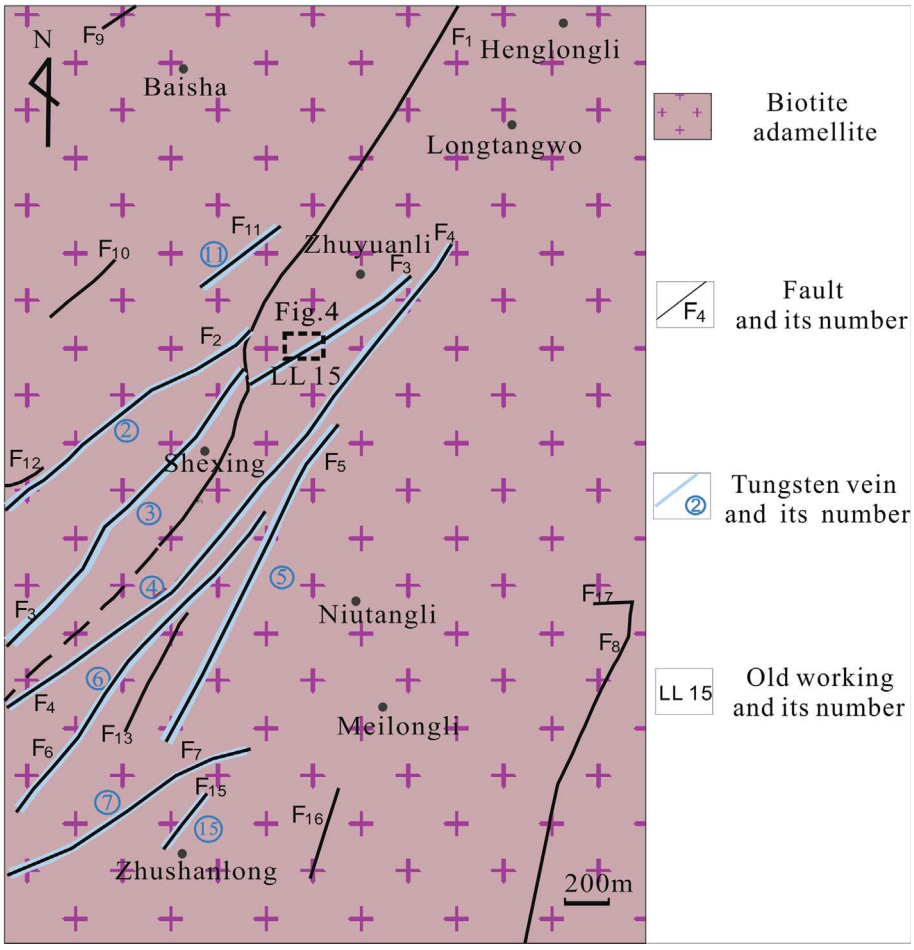

Fig. 3. Geological sketch map of the Zhuyuanli tungsten deposit (Modified from Hunan Institute of Geological Survey. 2006).

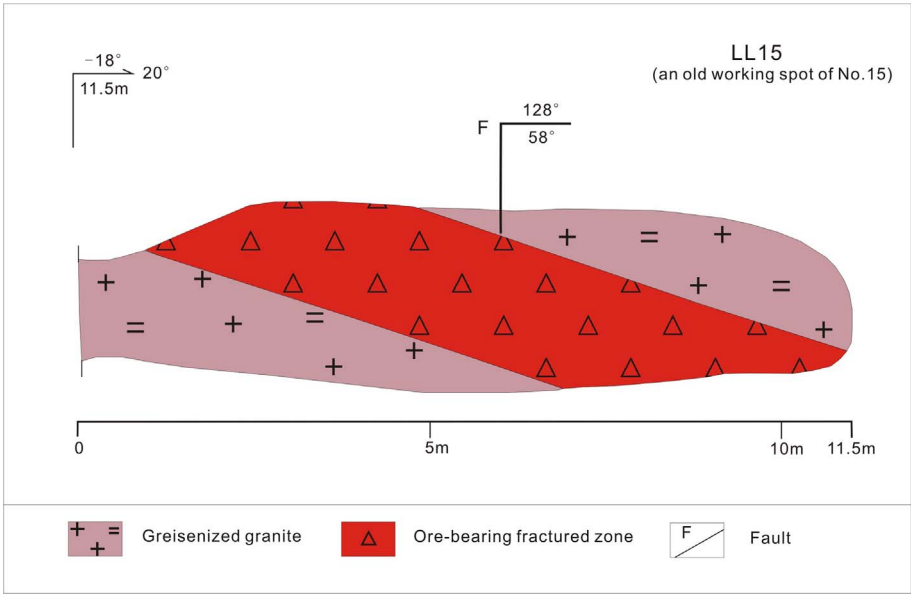

Fig. 4. An old working profile of the Zhuyuanli tungsten deposit (Modified from Hunan Institute of Geological Survey. 2006).

Services Ltd., Langfang, China.

4.1. *In situ* SIMS zircon U-Pb dating

To reveal their inner structures, all studied zircon grains were documented using transmitted and reflected light photomicrographs and cathodoluminescence (CL) images. Twenty-four zircon grains (Fig. 6) were chosen from the greisenized granite sample LY-9 of the Liuyuan deposit for SIMS U-Pb dating. Similarly, twenty-five zircon grains (Fig. 7) were selected from the greisen sample ZYL-1 of the Zhuyuanli deposit.

The U-Pb dating analyses were conducted with a Cameca IMS-1280

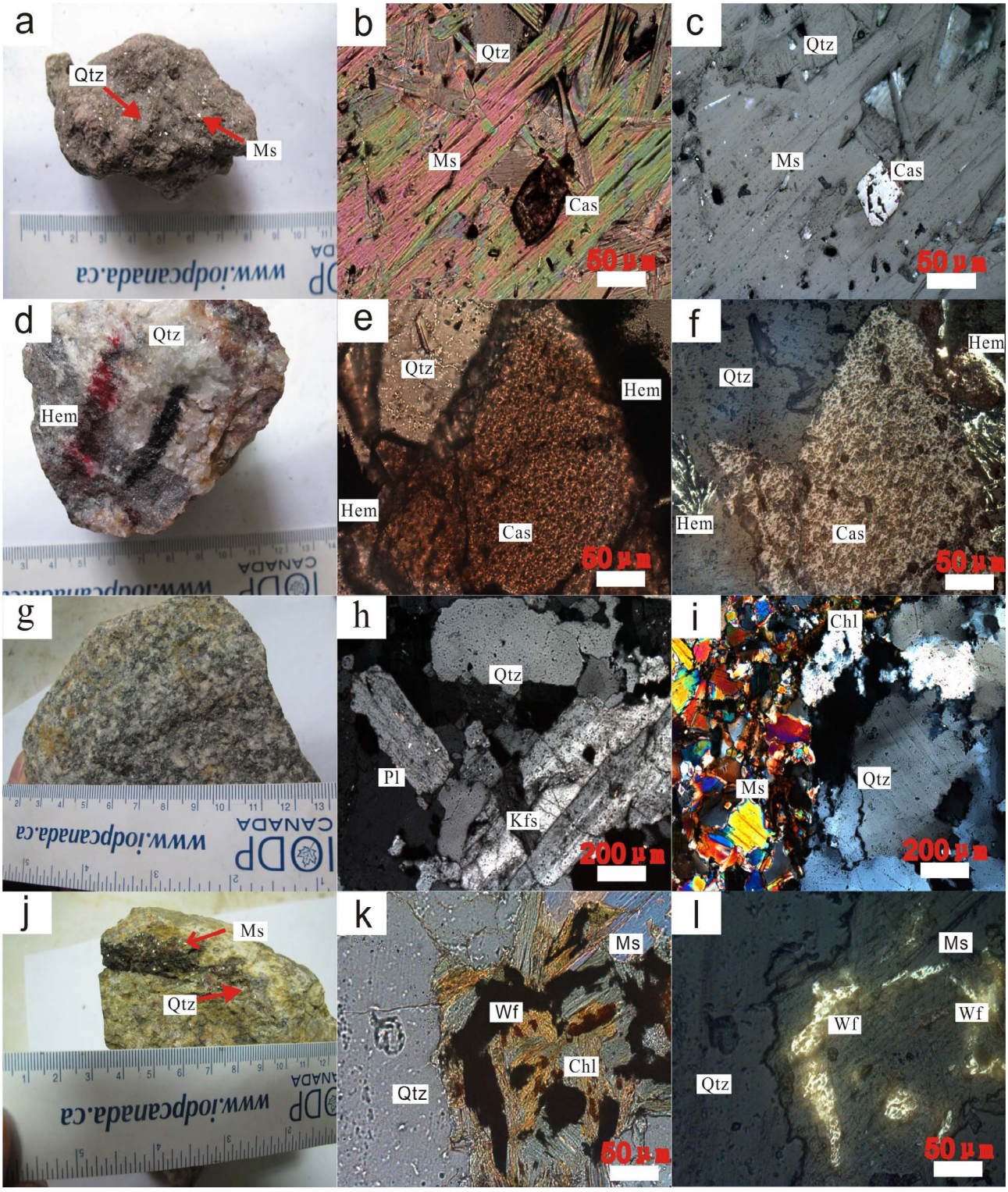

Fig. 5. Photographs of hand specimens and photomicrographs of granite, ore-bearing greisen and ore from the Liuyuan deposit, and ore-bearing greisenized granite from the Zhuyuanli deposit. (a), (b) and (c) cassiterite-bearing greisen from the Liuyuan tin deposit, cassiterite coexists with muscovite and quartz. (d), (e) and (f) quartz-cassiterite vein-type ore, quartz coexists with cassiterite and hematite. (g) and (h) granite from the Liuyuan tin deposit and with greisen alteration and chloritizationi). (j), (k) and (l) wolframite-bearing greisenized granite from the Zhuyuanli tungsten deposit, wolframite coexists with quartz, muscovite and chlorite. Abbreviations: Ms = muscovite; Qtz = quartz; Cas = cassiterite; Wf = wolframite; Pl = plagioclase; Kfs = K-feldspar; Chl = chlorite; Hem = hematite.

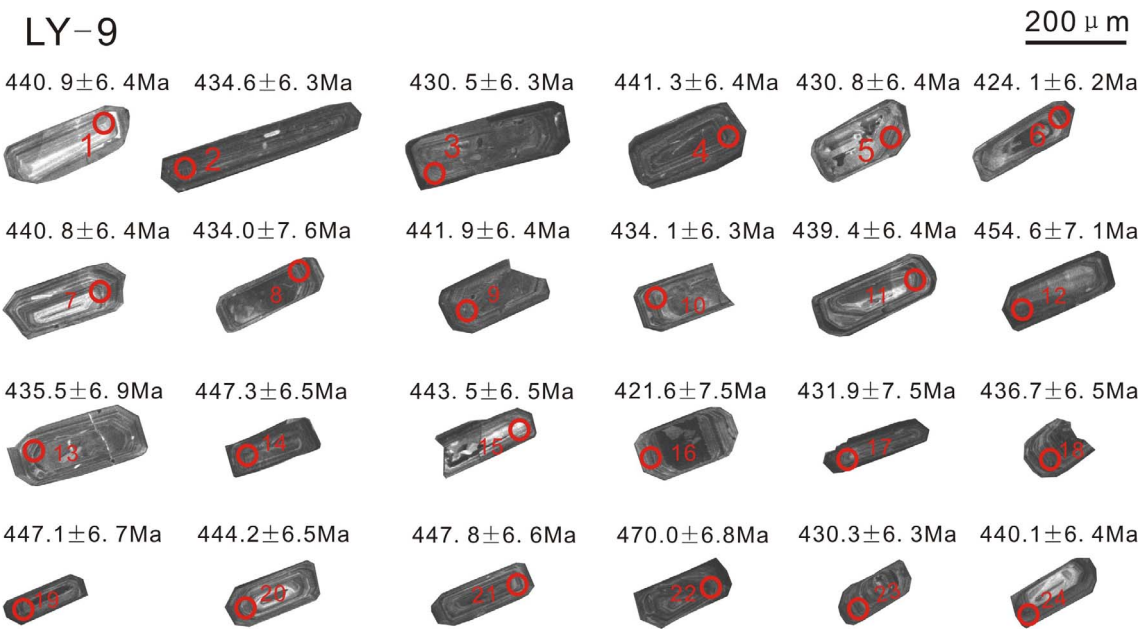

Fig. 6. Cathodoluminescence (CL) images of analysed zircons separated from greisen samples of the biotite granite in the Liuyuan deposit.

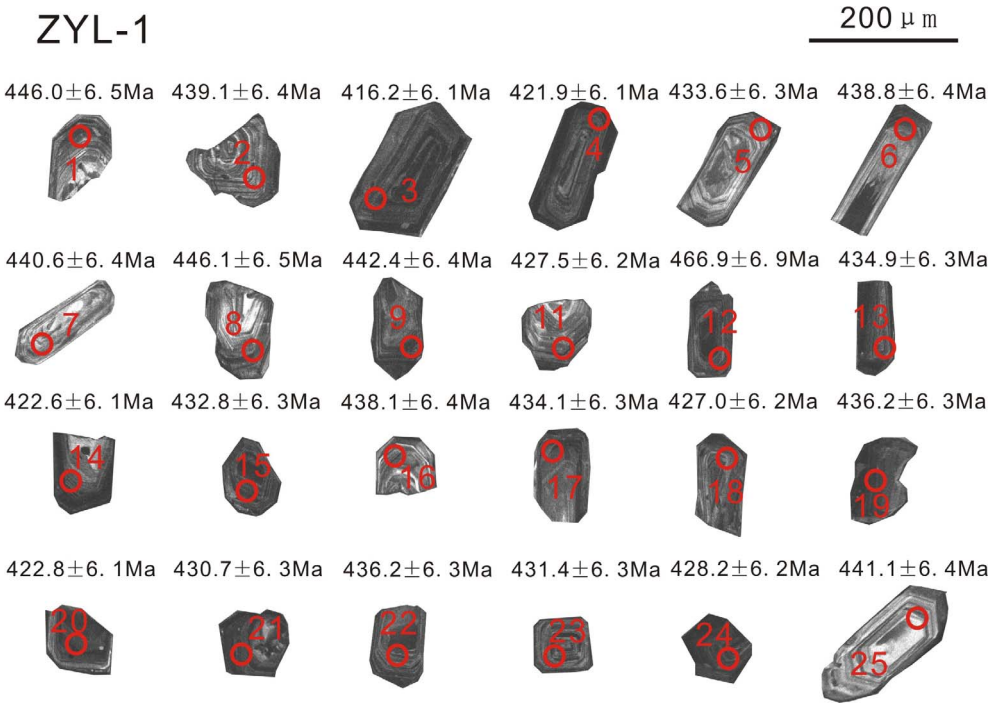

Fig. 7. Cathodoluminescence (CL) images of analysed zircons separated from greisenized granite samples in the Zhuyuanli deposit.

HR SIMS at the Institute of Geology and Geophysics, Chinese Academy of Sciences in Beijing. Description of this instrument and the analytical procedure can be found in Li et al. (2009). The brief summary presented here was provided by the laboratory. The primary O_2^- ion beam spot was approximately 20 × 30 μm in size. Positive secondary ions were extracted with a 10 kV potential. In the secondary ion beam optics, a 60 eV energy window was used, together with a mass resolution of ca. 5400 (at 10% peak height), to separate Pb peaks from isobaric interferences. A single electron multiplier was used in ion-counting mode to measure secondary ion beam intensities in peak-jumping mode. Analyses of the standard zircon Plesovice were interspersed with those of unknown grains. Each measurement consisted of 7 cycles. The Pb/U calibration was performed relative to the zircon standard Plesovice ($^{206}Pb/^{238}U$ age = 337 Ma, Sláma et al., 2008); U and Th concentrations were calibrated against those of the zircon standard 91,500 (Th = 29 ppm; U = 81 ppm, Wiedenbeck et al., 1995). A long-term uncertainty of 1.5% (1s RSD) for $^{206}Pb/^{238}U$ measurements of the standard zircons was propagated to the unknowns (Li et al., 2010),

Table 1
SIMS zircon U–Pb data from the greisen sample LY-9 and greisenized granite sample ZYL-1 from the Liuyuan deposit and Zhuyuanli deposit, respectively.

Sample spot	Concentration		Th/U	$^{206}Pb/^{204}Pb$ measured	Isotopic ratios and σ errors						Corrected ages and σ errors (Ma)					
	U(ppm)	Th(ppm)			$^{207}Pb/^{235}U$	σ	$^{206}Pb/^{238}U$	σ	$^{207}Pb/^{206}Pb$	σ	$^{207}Pb/^{235}U$	σ	$^{206}Pb/^{238}U$	σ	$^{207}Pb/^{206}Pb$	σ
LY-9-1	369	149	0.403	23,999	0.54773	1.81	0.0708	1.51	0.05611	1.01	443.5	6.5	440.9	6.4	456.9	22.3
LY-9-2	1179	340	0.288	26,484	0.53511	1.71	0.0697	1.51	0.05565	0.80	435.2	6.1	434.6	6.3	438.3	17.8
LY-9-3	1167	278	0.238	23,214	0.53262	1.61	0.0691	1.51	0.05593	0.55	433.5	5.7	430.5	6.3	449.6	12.3
LY-9-4	1656	568	0.343	35,952	0.54231	1.77	0.0709	1.50	0.05551	0.95	439.9	6.4	441.3	6.4	432.8	21.0
LY-9-5	1057	298	0.282	9794	0.52162	1.70	0.0691	1.53	0.05474	0.74	426.2	5.9	430.8	6.4	401.8	16.5
LY-9-6	1315	469	0.357	15,732	0.52022	1.64	0.0680	1.50	0.05548	0.65	425.3	5.7	424.1	6.2	431.5	14.4
LY-9-7	1397	303	0.217	36,868	0.54477	1.57	0.0708	1.50	0.05582	0.45	441.6	5.6	440.8	6.4	445.3	9.9
LY-9-8	1605	481	0.300	7378	0.53433	2.11	0.0696	1.80	0.05565	1.10	434.7	7.5	434.0	7.6	438.3	24.3
LY-9-9	1164	377	0.324	25,760	0.54983	1.64	0.0710	1.50	0.05620	0.64	444.9	5.9	441.9	6.4	460.2	14.2
LY-9-10	1421	452	0.318	13,941	0.53337	2.00	0.0697	1.51	0.05554	1.31	434.0	7.1	434.1	6.3	433.9	28.9
LY-9-11	2045	708	0.346	40,353	0.54196	1.74	0.0705	1.51	0.05573	0.87	439.7	6.2	439.4	6.4	441.5	19.1
LY-9-12	2516	603	0.240	13,819	0.55976	1.66	0.0731	1.62	0.05556	0.36	451.4	6.1	454.6	7.1	434.8	8.0
LY-9-13	1160	358	0.309	18,774	0.53862	1.81	0.0699	1.63	0.05589	0.78	437.5	6.5	435.5	6.9	448.0	17.3
LY-9-14	1797	438	0.244	22,008	0.55793	1.62	0.0718	1.51	0.05632	0.58	450.2	5.9	447.3	6.5	465.1	12.8
LY-9-15	1257	395	0.314	8388	0.54639	1.77	0.0712	1.51	0.05564	0.92	442.6	6.4	443.5	6.5	438.0	20.4
LY-9-16	1265	425	0.336	3150	0.51909	2.53	0.0676	1.84	0.05571	1.74	424.5	8.8	421.6	7.5	440.8	38.2
LY-9-17	1526	469	0.308	2580	0.50805	2.24	0.0693	1.79	0.05317	1.34	417.1	7.7	431.9	7.5	336.3	30.2
LY-9-18	1106	327	0.296	20,191	0.54030	1.78	0.0701	1.55	0.05591	0.89	438.6	6.4	436.7	6.5	448.9	19.6
LY-9-19	2222	648	0.292	22,048	0.55206	1.69	0.0718	1.56	0.05576	0.67	446.3	6.1	447.1	6.7	442.6	14.8
LY-9-20	874	288	0.330	36,510	0.54713	1.66	0.0713	1.52	0.05563	0.67	443.1	6.0	444.2	6.5	437.6	14.9
LY-9-21	884	275	0.310	1722	0.55580	2.33	0.0719	1.52	0.05604	1.76	448.8	8.5	447.8	6.6	453.9	38.7
LY-9-22	1650	482	0.292	34,197	0.58655	1.59	0.0756	1.50	0.05624	0.53	468.7	6.0	470.0	6.8	461.9	11.8
LY-9-23	1037	297	0.287	10,386	0.52308	1.77	0.0690	1.50	0.05496	0.94	427.2	6.2	430.3	6.3	410.4	20.8
LY-9-24	933	279	0.299	37,240	0.54432	1.63	0.0706	1.50	0.05588	0.64	441.3	5.9	440.1	6.4	447.6	14.2
ZYL-1-1	2426	773	0.318	52,868	0.55113	1.52	0.0716	1.50	0.05579	0.21	445.7	5.5	446.0	6.5	444.2	4.6
ZYL-1-2	1431	557	0.389	16,884	0.54474	1.52	0.0705	1.50	0.05605	0.26	441.5	5.5	439.1	6.4	454.4	5.8
ZYL-1-3	3715	896	0.241	1223	0.50377	2.11	0.0667	1.50	0.05478	1.48	414.2	7.2	416.2	6.1	403.4	32.8
ZYL-1-4	1512	597	0.395	3661	0.51061	1.66	0.0676	1.50	0.05475	0.72	418.9	5.7	421.9	6.1	401.9	16.1
ZYL-1-5	1229	449	0.365	75,724	0.53266	1.54	0.0696	1.50	0.05552	0.33	433.6	5.4	433.6	6.3	433.4	7.4
ZYL-1-6	1657	518	0.313	91,842	0.54107	1.52	0.0704	1.50	0.05571	0.25	439.1	5.4	438.8	6.4	440.9	5.5
ZYL-1-7	1335	459	0.344	84,881	0.54243	1.53	0.0707	1.50	0.05561	0.28	440.0	5.5	440.6	6.4	436.9	6.3
ZYL-1-8	1687	574	0.340	33,153	0.55030	1.53	0.0717	1.50	0.05570	0.31	445.2	5.5	446.1	6.5	440.6	6.8
ZYL-1-9	2377	531	0.223	44,624	0.54474	1.53	0.0710	1.50	0.05562	0.32	441.5	5.5	442.4	6.4	437.1	7.1
ZYL-1-10	1565	681	0.435	306	0.52503	3.52	0.0685	1.50	0.05561	3.18	428.5	12.4	427.0	6.2	436.9	69.3
ZYL-1-11	1280	486	0.379	47,651	0.52580	1.55	0.0686	1.51	0.05562	0.37	429.0	5.4	427.5	6.2	437.1	8.3
ZYL-1-12	2631	470	0.179	54,172	0.58313	1.54	0.0751	1.52	0.05630	0.23	466.5	5.8	466.9	6.9	464.4	5.2
ZYL-1-13	1594	595	0.373	8072	0.52942	1.54	0.0698	1.50	0.05501	0.34	431.4	5.4	434.9	6.3	412.8	7.6
ZYL-1-14	1186	302	0.255	14,641	0.51438	1.58	0.0678	1.50	0.05506	0.51	421.4	5.5	422.6	6.1	414.6	11.3
ZYL-1-15	1947	715	0.367	44,600	0.53369	1.53	0.0694	1.50	0.05574	0.25	434.3	5.4	432.8	6.3	442.0	5.6
ZYL-1-16	1245	553	0.444	63,493	0.53954	1.53	0.0703	1.50	0.05564	0.32	438.1	5.5	438.1	6.4	438.1	7.1
ZYL-1-17	1300	367	0.282	52,728	0.53324	1.53	0.0697	1.50	0.05552	0.31	434.0	5.4	434.1	6.3	433.2	6.8
ZYL-1-18	1897	832	0.439	7771	0.52202	1.56	0.0685	1.50	0.05529	0.41	426.5	5.4	427.0	6.2	424.0	9.0
ZYL-1-19	1855	501	0.270	26,453	0.53411	1.52	0.0700	1.50	0.05533	0.26	434.5	5.4	436.2	6.3	425.5	5.7
ZYL-1-20	2094	611	0.292	17,290	0.51779	1.53	0.0678	1.50	0.05541	0.28	423.7	5.3	422.8	6.1	428.7	6.3
ZYL-1-21	1603	529	0.330	40,501	0.52735	1.54	0.0691	1.50	0.05536	0.35	430.1	5.4	430.7	6.3	426.8	7.8
ZYL-1-22	1408	462	0.328	185,918	0.53515	1.53	0.0700	1.50	0.05544	0.27	435.2	5.4	436.2	6.3	430.1	6.0
ZYL-1-23	1749	1084	0.620	93,565	0.52853	1.53	0.0692	1.50	0.05538	0.28	430.8	5.4	431.4	6.3	427.7	6.1
ZYL-1-24	2201	829	0.377	91,648	0.52475	1.52	0.0687	1.50	0.05541	0.22	428.3	5.3	428.2	6.2	428.7	4.9
ZYL-1-25	912	174	0.191	33,371	0.53937	1.55	0.0708	1.50	0.05523	0.38	438.0	5.5	441.1	6.4	421.5	8.5

although the measured $^{206}Pb/^{238}U$ error in a specific session was generally ≤1% (1s RSD). The measured compositions were corrected for common Pb using non-radiogenic ^{204}Pb. These corrections are sufficiently small as to be insensitive to the choice of the common Pb composition, and an average of present-day crustal composition (Stacey and Kramers, 1975) is used for the common Pb assuming that the common Pb is largely surface contamination introduced during sample preparation. Data reduction was carried out using the Isoplot/Ex v. 2.49 program (Ludwig, 2001). Uncertainties on individual analyses in data tables are reported at the 1σ level; concordia U-Pb ages are quoted with a 95% confidence interval, except where otherwise noted.

To monitor the external uncertainties in the SIMS U-Pb zircon dating calibrated against the Plesovice standard, an in-house zircon standard Qinghu was alternately analysed as an unknown together with other unknown zircons. Twenty-two measurements of the Qinghu zircon yielded a concordia age of 160 ± 1 Ma, which is identical within error to the recommended value of 159.5 ± 0.2 Ma (Li et al., 2013b).

4.2. *Muscovite ^{40}Ar-^{39}Ar dating*

Muscovite grains, which are intergrown with cassiterite (Fig. 5b, c) in the greisen sample LY-11 from the Liuyuan deposit, were selected for Ar-Ar dating. Additionally, muscovite grains intergrown with wolframite (Fig. 5 k, l) in the greisenized granite sample ZYL-1 from the Zhuyuanli tungsten deposit were selected for Ar-Ar dating. The

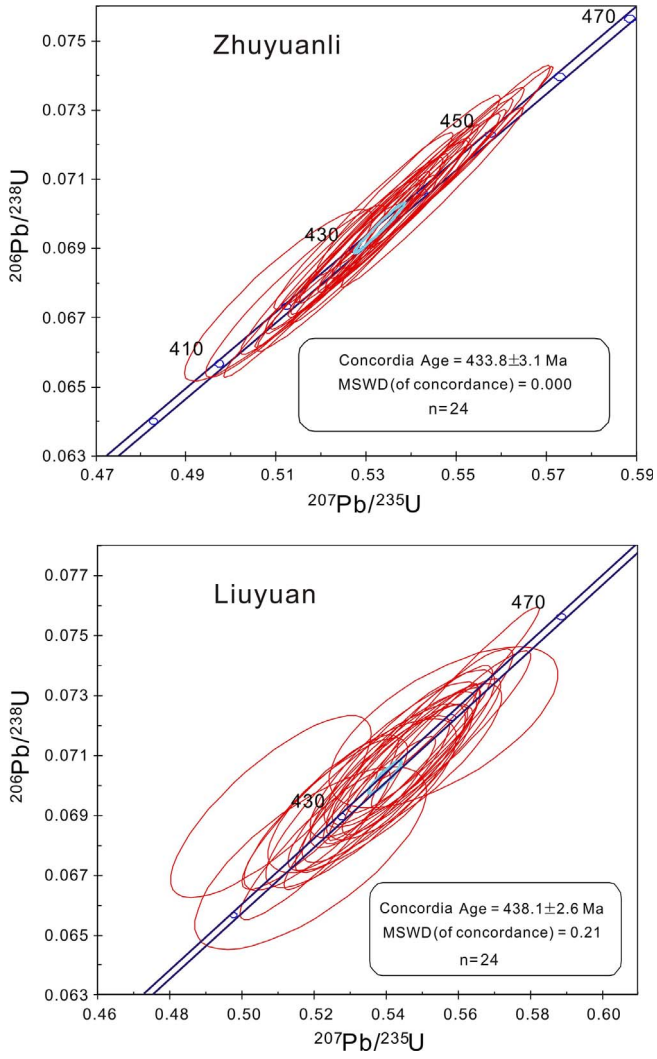

Fig. 8. SIMS zircon U-Pb concordia diagram for the greisen sample of the biotite granite from the Liuyuan deposit, and the greisenized granite sample from the Zhuyuanli deposit.

analysed muscovite grains were repeatedly cleaned in an ultrasonic bath using ethanol. The samples were then sealed in separate quartz vials for subsequent irradiation at the Chinese Institute of Atomic Energy. The grains were irradiated for 1444 min, and the neutron flux was approximately 2.6×10^{13} n cm^{-2} S^{-1}. The Fangshan biotite standard (ZBH-25) was used to monitor the neutron flux. After irradiation, the samples underwent stepwise heating in a graphite furnace. The mass analysis was conducted with a Helix C Plus multi-collector noble gas mass spectrometer at the Isotope Laboratory of the Institute of Geology, Chinese Academy of Geosciences. The detailed operation and data processing procedures were described by Chen et al. (2006).

5. Results

5.1. SIMS zircon U-Pb ages

The analysed zircon grains are generally colourless, transparent, euhedral and prismatic. The CL images show that most of these grains exhibit oscillatory magmatic zoning and range in length from 60 to 500 μm, with length/width ratios of 1–5. The abundances of U and Th obtained from all analysed zircon spots are presented in Table 1. The Th/U ratios of these grains, which range from 0.18 to 0.62, as well as their microscale oscillatory zoning, are typical features of magmatic zircons (Hoskin and Schaltegger, 2003). For sample LY-9, the data from all 24 spots are concordant and yield a $^{206}Pb/^{238}U$ concordia age of 438.1 ± 2.6 Ma (Fig. 8), which represents the crystallization age of the magmatic zircons in the greisen of the Liuyuan deposit. For sample ZYL-1, the ZYL-1-10 data were rejected due to their high common lead content. The remaining age data from the other 24 spots have a high concordance and yield a $^{206}Pb/^{238}U$ concordia age of 433.8 ± 3.1 Ma (Fig. 8), which represents the crystallization age of the magmatic zircons from the greisenized granite in the Zhuyuanli deposit. The similar zircon U-Pb age data obtained from the greisen and greisenized granite samples from these two deposits indicate that the Guidong batholith was emplaced at ~438.1–433.8 Ma. The new SIMS U-Pb age of the Guidong granite is consistent with the previous LA-ICP-MS zircon U-Pb age of the Guidong granite (432 ± 2 Ma; Zhao and Chen, 2013) within analytical uncertainty.

5.2. Muscovite Ar-Ar ages

The analytical data of the two samples from the Liyuan deposit (LY-11) and the Zhuyuanli deposit (ZYL-1) are displayed in Table 2 and 3, and they are illustrated in Fig. 9. The ^{40}Ar-^{39}Ar muscovite steps of sample LY-11 yield a well-defined plateau age of 153.10 ± 0.96 Ma (MSDW = 0.37), an isochron age of 153.2 ± 1.5 Ma (MSWD = 1.4), and an inverse isochron age of 152.8 ± 1.6 Ma (MSWD = 28). The three age data are in fairly good agreement, which means that the

Table 2
^{40}Ar-^{39}Ar data for muscovite from sample LY-11 in the Liuyuan deposit.

T (°C)	$(^{40}Ar/^{39}Ar)_m$	$(^{36}Ar/^{39}Ar)_m$	$(^{37}Ar_0/^{39}Ar)_m$	$(^{38}Ar/^{39}Ar)_m$	^{40}Ar (%)	F	$^{39}Ar(\times10^{-14}mol)$	^{39}Ar(Cum.)(%)	Age (Ma)	± 1σ (Ma)
680	84.6110	0.1864	0.0000	0.0483	34.89	29.5191	0.12	0.59	119.1	2.5
760	63.7729	0.0918	0.0000	0.0267	57.45	36.6406	0.23	1.77	146.6	2.4
800	68.5473	0.1068	0.0120	0.0323	53.95	36.9800	0.29	3.25	147.9	1.9
850	46.2822	0.0285	0.1522	0.0184	81.80	37.8646	0.85	7.63	151.3	1.5
900	38.8948	0.0027	0.0000	0.0132	97.93	38.0892	3.77	27.04	152.2	1.5
930	38.7277	0.0010	0.0000	0.0128	99.21	38.4216	2.88	41.84	153.5	1.5
960	38.7399	0.0010	0.0116	0.0128	99.27	38.4556	3.82	61.52	153.6	1.5
990	38.9246	0.0011	0.0437	0.0128	99.17	38.6021	3.38	78.89	154.2	1.5
1030	39.5981	0.0037	0.0671	0.0130	97.23	38.5035	1.39	86.05	153.8	1.5
1070	39.8389	0.0048	0.1429	0.0137	96.43	38.4230	1.14	91.90	153.5	1.5
1120	39.8518	0.0048	0.1798	0.0140	96.43	38.4335	0.98	96.94	153.5	1.5
1200	41.8018	0.0117	0.0898	0.0151	91.75	38.3578	0.44	99.20	153.2	1.5
1400	62.4408	0.0827	0.4341	0.0261	60.90	38.0374	0.16	100.00	152.0	1.7

LY-11, sample weight = 14.17 mg, J = 0.002311, F = $^{40}Ar^*/^{39}Ar$, is the ratio of radiogenic Argon40 and Argon39.

Table 3
^{40}Ar-^{39}Ar data for muscovite from sample ZYL-1 in the Zhuyuanli deposit.

T (°C)	$(^{40}Ar/^{39}Ar)_m$	$(^{36}Ar/^{39}Ar)_m$	$(^{37}Ar_0/^{39}Ar)_m$	$(^{38}Ar/^{39}Ar)_m$	^{40}Ar (%)	F	$^{39}Ar(\times10^{-14}mol)$	^{39}Ar(Cum.)(%)	Age (Ma)	± 1σ (Ma)
600	69.7681	0.1960	0.0239	0.0433	16.99	11.8565	0.04	0.13	84	15
700	30.2401	0.0355	0.0000	0.0180	65.30	19.7482	0.36	1.19	138.0	2.2
750	27.9858	0.0227	0.0149	0.0162	76.00	21.2682	0.70	3.25	148.2	1.6
800	26.0153	0.0153	0.0089	0.0150	82.60	21.4894	1.30	7.11	149.7	1.5
830	27.3585	0.0198	0.0498	0.0158	78.56	21.4924	1.34	11.08	149.7	1.5
860	25.5343	0.0130	0.0069	0.0146	84.98	21.6994	2.60	18.78	151.1	1.5
890	23.4543	0.0049	0.0275	0.0129	93.75	21.9898	1.20	22.33	153.0	1.6
920	22.6678	0.0030	0.0057	0.0127	96.07	21.7767	5.25	37.86	151.6	1.5
950	22.8557	0.0037	0.0067	0.0130	95.25	21.7700	5.52	54.20	151.6	1.5
980	23.3775	0.0052	0.0047	0.0131	93.46	21.8489	4.82	68.48	152.1	1.5
1020	23.7517	0.0062	0.0092	0.0134	92.24	21.9095	4.71	82.43	152.5	1.5
1070	24.1993	0.0077	0.0157	0.0137	90.63	21.9326	4.63	96.13	152.7	1.5
1130	24.7860	0.0097	0.0347	0.0139	88.46	21.9270	1.21	99.71	152.6	1.5
1400	198.3878	0.5913	0.0000	0.1195	11.93	23.6612	0.10	100.00	164.1	6.4

ZYL-1, sample weight = 12.52 mg, J = 0.004026, F = $^{40}Ar^*/^{39}Ar$, is the ratio of radiogenic Argon40 and Argon39.

plateau age of 153.10 ± 0.96 Ma can represent the crystallization age of muscovite. Similarly, the plateau age (151.64 ± 0.96 Ma), isochron age (152.8 ± 1.8 Ma) and inverse isochron age (152.17 ± 1.7 Ma) of the Zhuyuanli muscovite sample are in good agreement with each other within the applicable analytical uncertainty. Therefore, the plateau age of 151.64 ± 0.96 Ma is estimated to represent the crystallization age of muscovite in the Zhuyuanli deposit.

6. Discussion

6.1. Timing and ore genesis of the Liuyuan and Zhuyuanli W-Sn deposits

In recent years, mineral exploration studies in the Penggongmiao-Guidong area have revealed a series of W-Sn deposits and occurrences around the two Caledonian Penggongmiao and Guidong granite batholiths. The W-Sn mineralization in this area has long been believed to have formed during the Caledonian (Qiao et al., 2011; Li et al., 2013a). However, the timing of the formation of the regional W-Sn mineralization is still unclear due to the lack of age data constraining the timing of the ore genesis in these ore deposits. The detailed geological investigations of the Liuyuan tin and Zhuyuanli tungsten deposits (Figs. 2 and 3) show that almost all of the orebodies are controlled by the well-developed regional NE- and NNE-trending faults. In the Liuyuan tin deposit, the granites on both sides of the ore-bearing NE-trending faults experienced intensive greisen alteration (Fig. 2). However, similar degrees of greisen alteration are uncommon in the rest of the mining area, farther from the ore-bearing faults (Fig. 2). Similarly, in the Zhuyuanli tungsten deposit (Fig. 3), the ore veins that are primarily hosted in the regional NE- and NNE-trending faults are generally accompanied by large-scale greisen alteration. The greisen bodies in the Liuyuan and Zhuyuanli W-Sn deposits are well controlled by the fractures, in contrast to the massive greisen occurring in the apical portion of ore-causative granite (Taylor, 1979; Lehmann, 1990). Our new high-precision zircon SIMS U-Pb dating data show that the Guidong granites from these two deposits consistently record Caledonian emplacement ages, with ages of 433.8 ± 3.1 Ma in the Zhuyuanli area and 438.1 ± 2.6 Ma in the Liuyuan area. The $^{40}Ar/^{39}Ar$ plateau age of muscovite (153.10 ± 0.96 Ma) in the greisen of the Liuyuan deposit is highly consistent with the $^{40}Ar/^{39}Ar$ plateau age of muscovite (151.64 ± 0.96 Ma) in the greisenized granite of the Zhuyuanli tungsten deposit; these are both clearly indicative of Late Jurassic W-Sn mineralization. Therefore, these W-Sn mineralization age data are distinct from the zircon SIMS U-Pb ages of their ore-hosting Caledonian granites. Combined with the results of detailed geological investigations, these remarkable age differences suggest that there is no genetic correlation between the granite batholith and regional W-Sn mineralization and that concealed Late Jurassic ore-related granites likely exist at depth in this area.

6.2. The W-Sn exploration potential of the Penggongmiao-Guidong area

The recent discovery of the world-class Dahutang supergiant tungsten deposit (Mao et al., 2015), the large Xitian tin deposit (Zhou et al., 2015), and the large Zhangjialong tungsten deposit (Qiao et al., 2011), all of which are hosted in or near granite batholiths in South China, has highlighted the mineral potential of the area surrounding the granitic batholiths in the Nanling Range and its adjacent region. In the Penggongmiao-Guidong area, the latest exploration revealed a series of W-Sn deposits and occurrences distributed around two regional batholiths (Fig. 1), including the Zhangjialong, Yangmeikeng and Zhenkou tungsten deposits which are located on the southern margin of the Penggongmiao batholith, and the Zhuyuanli tungsten deposit and the Liuyuan tin deposit which are located on the western margin of the Guidong batholith (Qiao et al., 2011; Li et al., 2013a). As these W-Sn deposits are always spatially linked to Caledonian granite batholiths, the regional prospecting strategy has focused on the Caledonian granites and their contact zones with pre-existing strata. Our highly precise muscovite Ar-Ar data indicate that both the Zhuyuanli tungsten and Liuyuan tin deposits formed during the Late Jurassic. Furthermore, these ore-formation ages in the Guidong area agree well with those of the Late Jurassic W-Sn mineralization related to granite stocks or apophyses in the Nanling Range (160–150 Ma; Yuan et al., 2008, 2012b; Peng et al., 2006; Hu et al., 2012; Hu and Zhou, 2012; Mao et al., 2008, 2013), which is one of the most significant ore-forming events in this region. This important episode of granite emplacement and mineralization is evidenced by a series of supergiant and giant W-Sn deposits, such as the Xianghualing Sn deposit (Yuan et al., 2007), the Shizhuyuan W-Sn-Mo-Bi deposit (Li et al., 1996), the Yaogangxian W deposit (Peng et al., 2006), the Hongqiling Sn deposit (Yuan et al., 2012a), the Jinchuantang Sn-Bi deposit (Liu et al., 2012), the Huangshaping Pb-Zn-W-Mo deposit (Yuan et al., 2014), and the Weijia W deposit (Zhao et al., 2016). Therefore, our high-precision ore-forming age data from the Liuyuan and Zhuyuanli deposits suggest that significant Late Jurassic W-Sn mineralization potential and related magmatism exist along the western margin of the Guidong batholith, where fault-related fractures have developed in the Penggongmiao-Guidong area.

7. Conclusions

(1) The results of muscovite Ar-Ar dating show that the Liuyuan tin deposit and the Zhuyuanli tungsten deposit formed at 153.10 ± 0.96 Ma and 151.64 ± 0.96 Ma, respectively. These ages are significantly younger than the zircon SIMS U-Pb ages of

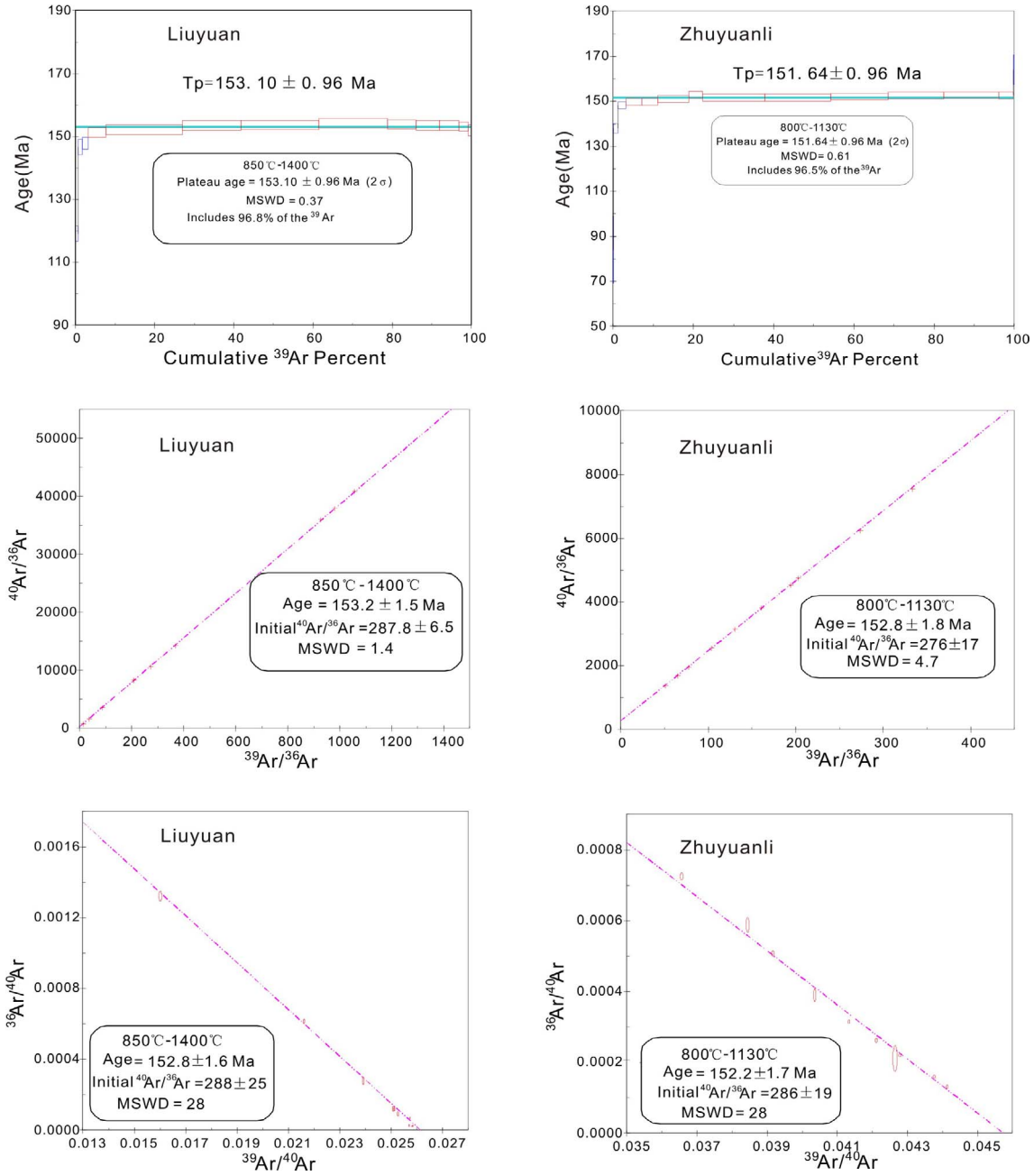

Fig. 9. Plateau, isochron and inverse isochron ^{40}Ar-^{39}Ar ages of muscovites from the greisen-type ores of the Liuyuan and Zhuyuanli deposits, respcetively.

their ore-hosting granites (438.1 ± 2.6 Ma, 433.8 ± 3.1 Ma). Combined with the results of a detailed geological investigation, these age data suggest that there is no genetic correlation between the granite batholith and regional W-Sn mineralization, and that concealed Late Jurassic ore-related granites likely exist at depth in this region.

(2) Our new high-precision geochronological data indicate that the ore-formation ages of the Liuyuan and Zhuyuanli deposits agree well with the W-Sn mineralization event of Late Jurassic in the Nanling Range, which suggests that there is significant potential for Late Jurassic W-Sn exploration along the western margin of the Guidong batholith in the Penggongmiao-Guidong area.

Acknowledgements

This work was financially supported jointly by the National Key R&D Program of China (No. 2016YFC0600207, No. 2016YFC0600205), the National Nonprofit Institute Research Grant of CAGS (YYWF201711) and the National Natural Science Foundation of China (Nos. 41373047, 41672095). We thank two anonymous referees for the comments and suggestions which are very helpful in improving this paper.

References

Chen, P.R., Hua, R.M., Zhang, B.T., 2002. Early Yanshanian post-orogenic granitoids in the Nanling region: petrological constraints and geodynamic settings. Sci. China (Series D) 32, 279–289 (in Chinese).

Chen, W., Zhang, Y., Jin, G.S., Zhang, Y.Q., Wang, Q.L., 2006. Late Cenozoic episodic uplifting in southeastern part of the Tibetan Plateau: evidence from Ar–Ar thermochronology. Acta Petrol. Sin. 22, 867–872 (in Chinese with English abstract).

Chen, J., Lu, J.J., Chen, W.F., Wang, R.C., Ma, D.S., Zhu, J.C., Zhang, W.L., Ji, J.F., 2008. W-Sn-Nb-Ta-Bearing granites in the Nanling range and their relationship to

metallogengesis. Geolog. J. China Univ. 4, 459–473 (in Chinese with English abstract).
Chen, J., Wang, R.C., Zhu, J.C., Lu, J.J., Ma, D.S., 2013. Multiple-aged granitoids and related tungsten-tin mineralization in the Nanling Range, South China. Sci. China Earth Sci. 56, 2045–2055.
Hoskin, P.W., Schaltegger, U., 2003. The composition of zircon and igneous and metamorphic petrogenesis. Rev. Mineral. Geochem. 53, 27–62.
Hu, R.Z., Zhou, M.F., 2012. Multiple Mesozoic mineralization events in South China—an introduction to the thematic issue. Miner. Deposita 47, 579–588.
Hu, R.Z., Wei, W.F., Bi, X.W., Peng, J.T., Qi, Y.Q., Wu, L.Y., Chen, Y.W., 2012. Molybdenite Re-Os and muscovite $^{40}Ar/^{39}Ar$ dating of the Xihuashan tungsten deposit, central Nanling district, South China. Lithos 150, 111–118.
Hua, R.M., 2005. Differences between rock-forming and related ore-forming times for the mesozoic granitoids of crust remelting types in the Nanling Range, South China, and its Geological Significance. Geolog. Rev. 51, 633–639 (in Chinese with English abstract).
Hua, R.M., Zhang, W.L., Chen, P.R., Zhai, W., Li, G.L., 2013. Relationship between Caledonian granitoids and large-scale mineralization in South China. Geolog. J. China Univ. 19, 1–11 (in Chinese with English abstract).
Lehmann, B., 1990. Metallogeny of Tin. Lecture Notes in Earth Sciences, vol. 32 Berlin Springer Verlag.
Li, H.Y., Mao, J.W., Sun, Y.L., Zou, X.Q., He, H.L., Du, A.D., 1996. Re-Os isotopic chronology of molybdenites in the Shizhuyuan polymetallic tungsten deposit, southern Hunan. Geolog. Rev. 42, 261–267 (in Chinese with English Abstract).
Li, X.H., Liu, Y., Li, Q.L., Guo, C.H., Chamberlain, K.R., 2009. Precise determination of Phanerozoic zircon Pb/Pb age by multi-collector SIMS without external standardization. Geochem. Geophys. Geosyst. 10.
Li, Q.L., Li, X.H., Liu, Y., Tang, G.Q., Yang, J.H., Zhu, W.G., 2010. Precise U-Pb and Pb-Pb dating of Phanerozoic baddeleyite by SIMS with oxygen flooding technique. J. Anal. At. Spectrom. 25, 1107–1113.
Li, S.Q., Lan, X.M., Deng, S.H., Chen, S.F., Wang, F.Y., Li, C.B., Huang, G.H., 2013a. Metallogenic geological characteristics of Caledonian tungsten deposits in Zhenkou area of Hunan Province and ore-prospecting orientation. Miner. Deposits 32, 405–414 (in Chinese with English Abstract).
Li, X.H., Tang, G.Q., Gong, B., Yang, Y.H., Hou, K.J., Hu, Z.C., Li, Q.L., Liu, Y., Li, W.X., 2013b. Qinghu zircon: A working reference for microbeam analysis of U-Pb age and Hf and O isotopes. Chin. Sci. Bull. 58, 4647–4654.
Liu, X.F., Yuan, S.D., Wu, S.H., 2012. Re-Os dating of the molybdenite from the Jinchuantang tin-bismuth deposit in Hunan Province and its geological significance. Acta Petrol. Sin. 28, 39–51 (in Chinese with English abstract).
Ludwig, K.R., 2001. User's manual for isoplot/ex, v2.49, a geochronological toolkit for Microsoft Excel. Geochronolog. Center Sp. Publ. 1–58.
Mao, J.W., Xie, G.Q., Guo, C.L., Chen, Y.C., 2007. Large-scale tungsten-tin mineralization in the Nanling area, South China: metallogenic ages and corresponding geodynamic processes. Acta Petrol Sin. 23, 2329–2338 (in Chinese with English abstract).
Mao, J.W., Xie, G.Q., Guo, C.L., Yuan, S.D., Cheng, Y.B., Chen, Y.C., 2008. Spatial-temporal distribution of Mesozoic ore deposits in South China and their metallogenic setting. Geolog. J. China Univ. 14, 510–526 (in Chinese with English Abstract).
Mao, J.W., Cheng, Y.B., Chen, M.H., Franco, P., 2013. Major types and time-space distribution of Mesozoic ore deposits in South China and their geodynamic settings. Miner. Deposita 48, 267–294.
Mao, Z.H., Liu, J.J., Mao, J.W., Deng, J., Zhang, F., Meng, X.Y., Xiong, B.K., Xiang, X.K., Luo, X.H., 2015. Geochronology and geochemistry of granitoids related to the giant Dahutang tungsten deposit, middle Yangtze River region, China: implications for petrogenesis, geodynamic setting, and mineralization. Gondwana Res. 28, 816–836.
Peng, J.T., Zhou, M.F., Hu, R.Z., Shen, N.P., Yuan, S.D., Bi, X.W., Du, A.D., Qu, W.J., 2006. Precise molybdenite Re-Os and mica Ar-Ar dating of the Mesozoic Yaogangxian tungsten deposit, central Nanling district. South China. Miner Deposita. 41, 661–669.
Qiao, Y.S., Wang, F.Y., Hou, M.S., Lei, Z.H., Li, C.B., 2011. Geological characteristics of Zhangjialong tungsten deposit, Hunan Province. Geol. Miner. Resour. South China 27, 125–131 (in Chinese with English Abstract).
Shu, L.S., Wang, D.Z., 2006. Comparison studies on the basin-range tectonics in northwest America and southeast China. Geol. J. Chinese Univ. 12, 1–13 (in Chinese with English abstract).
Sláma, J., Košler, J., Condon, D.J., Crowley, J.L., Gerdes, A., Hanchar, J.M., Schaltegger, U., 2008. Plešovice zircon—a new natural reference material for U-Pb and Hf isotopic microanalysis. Chem. Geol. 249, 1–35.
Stacey, J.S., Kramers, J.D., 1975. Approximation of terrestrial lead isotope evolution by a two-stage model. Earth Planet. Sci. Lett. 26, 207–221.
Taylor, R.G., 1979. Geology of tin deposits. Dev. Econ. Geol. 11.
Wiedenbeck, M.A.P.C., Alle, P., Corfu, F., Griffin, W.L., Meier, M., Oberli, F.V., Spiegel, W., 1995. Three natural zircon standards for U-Th-Pb, Lu-Hf, trace element and REE analyses. Geostand. Geoanal. Res. 19, 1–23.
Yuan, S.D., Peng, J.T., Shen, N.P., Hu, R.Z., Dai, T.M., 2007. ^{40}Ar-^{39}Ar isotopic dating of the Xianghualing Sn-polymetallic orefield in southern Hunan, China and its geological implications. Acta Geologica Sinica (English Edition) 81, 278–286.
Yuan, S.D., Peng, J.T., Hu, R.Z., Li, H.M., Shen, N.P., Zhang, D.L., 2008. A precise U-Pb age on cassiterite from the Xianghualing tin-polymetallic deposit (Hunan, South China). Miner. Deposita 43, 375–382.
Yuan, S.D., Peng, J.T., Hao, S., Li, H.M., Geng, J.Z., Zhang, D.L., 2011. In situ LA-MC-ICP-MS and ID-TIMS U-Pb geochronology of cassiterite in the giant Furong tin deposit, Hunan Province, South China: new constraints on the timing of tin-polymetallic mineralization. Ore Geol. Rev. 43, 235–242.
Yuan, S.D., Liu, X.F., Wang, X.D., Wu, S.H., Yuan, Y.B., Li, X.K., Wang, T.Z., 2012a. Geological characteristics and ^{40}Ar-^{39}Ar geochronology of the Hongqiling tin deposit in southern Hunan Province. Acta Petrol. Sin. 28, 3787–3797 (in Chinese with English abstract).
Yuan, S.D., Zhang, D.L., Shuang, Y., Du, A.D., Qu, W.J., 2012b. Re-Os dating of molybdenite from the Xintianling giant tungsten-molybdenum deposit in southern Hunan Province, China and its geological implications. Acta Petrologica Sinica. 28, 27–38 (in Chinese with English abstract).
Yuan, Y.B., Yuan, S.D., Chen, C.J., Huo, R., 2014. Zircon U-Pb ages and Hf isotopes of the granitoids in the Huangshaping mining area and their geological significance. Acta Petrologica Sinica. 30, 64–78 (in Chinese with English Abstract).
Zhao, Z.Y., Chen, B.F., 2013. Discussion on Geology of Guidong—Zhuguangshan Massif and U-Pb Age of Zircon. Gansu Metall. 35, 72–76 (in Chinese with English abstract).
Zhao, P.L., Yuan, S.D., Yuan, Y.B., 2016. Zircon LA-MC-ICP-MS U-Pb dating of the Xianglinpu granites from the Weijia tungsten deposit in southern Hunan Province and its implications for the Late Jurassic tungsten metallogenesis in the westernmost Nanling W-Sn metallogenic belt. Geol. China 43, 120–131 (in Chinese with English Abstract).
Zhou, Y., Liang, X.Q., Wu, S.C., Cai, Y.F., Liang, X.R., Shao, T.B., Wang, C., Fu, J.G., Jiang, Y., 2015. Isotopic geochemistry, zircon U-Pb ages and Hf isotopes of A-type granites from the Xitian W-Sn deposit, SE China: Constraints on petrogenesis and tectonic significance. J. Asian Earth Sci. 105, 122–139.